Synthesis, characterization and low temperature carbonation of mesoporous magnesium oxide

Sondes Hamdi, Laetitia Vieille, Kais Nahdi, Loïc Favergeon

Synthesis, characterization and low temperature carbonation of mesoporous magnesium oxide

Sondes Hamdi[1], Laetitia Vieille[2], Kais Nahdi[1], Loïc Favergeon[2]

[1]Laboratoire d'Application de la Chimie Aux Ressources et Substances Naturelles et à l'Environnement, Université de Carthage, Faculté des Sciences de Bizerte, 7021 Zarzouna, Bizerte, Tunisia
[2]Mines Saint-Etienne, Univ. Lyon, CNRS, UMR 5307 LGF, Centre SPIN, F-42023 Saint-Etienne, France

Abstract

A sample of MgO was successfully synthesized using thermal decomposition of hydromagnesite and compared to commercial material. The characterization of materials using XRD, SEM, BET and BJH methods showed that the thermal decomposition way led to rectangular mesoporous micro-sheets with high specific surface area of 100 m^2 g^{-1}. This porous magnesium oxide has been shown to be a potential candidate for CO_2 capture at low temperatures range (30 and 50° C), low pressures of CO_2 (P_{CO2} = 600 mbar) and in the presence of water vapor (P_{H2O} = 15 mbar). In these conditions our results show that 11% of MgO was converted to hydrated magnesium carbonate $MgCO_3.3H_2O$ after 8h of carbonation in a thermobalance, and reached 54% after 24h of carbonation using tube furnace. After carbonation hydration reaction pore size and surface area have noticeably changed.

Keywords: CO_2 capture, magnesium oxide, mesoporous, Nesquehonite, Thermogravimetric analysis

1. Introduction

The world total greenhouse gas (GHG) emissions are continuing to increase dramatically every decade. Currently, a large focus on removal of carbon dioxide, one of the greenhouse gases contributes to the global warming effects once accumulates into atmosphere. It is reported that CO_2 emissions were doubled from about 910 Gt CO_2 for the period 1750-1970 to about 2000 Gt CO_2 for 1750-2010, for this period it is noticeable that CO_2 emissions from industrial processes and fossil fuel combustion reached 78% of total GHG emissions [1], thus, specific measures should be taken to control CO_2 emissions.

In 1990 Seifritz introduced the mineral carbonation [2], from that, the concept of carbon dioxide capture and storage (CSS) has attracted the researcher's attention since it could be the best solution to remove CO_2 from natural gas and flue gas effluent.

In order to identify promising sorbents, Kumar et al. [3] have made a comparative study of CO_2 sorption properties for various oxides. Among seven candidates, magnesium oxide (MgO), calcium oxide (CaO), lithium zirconate (Li_2ZrO_3), calcium zirconate ($CaZrO_3$), barium zirconate ($BaZrO_3$), barium titanate ($BaTiO_3$) and barium silicate ($BaSiO_3$), the first two oxides (MgO and CaO) have the most attractive properties and this for two reasons.

The first one concerns the thermodynamic properties of both carbonation reaction (see Eqs. R1 and R2 for the CaO carbonation and MgO carbonation respectively) which show that CaO and MgO are able to establish a chemical bond with CO_2 to form stable carbonates. Furthermore, both reactions are exothermal which means that metal oxide can be fully regenerated by simple heating the carbonate.

$$CaO(s) + CO_2(g) \leftrightarrow CaCO_3(s) \quad \Delta_rH° = -179 \text{ kJ mol}^{-1} \text{ at } 298 \text{ K} \qquad (R1)$$

$MgO(s) + CO_2(g) \leftrightarrow MgCO_3(s)$ $\Delta_r H° = -118$ kJ mol^{-1} at 298 K (R2)

The second reason is that MgO and CaO are more abundant in the nature than the other metal oxides.

The use of CaO as a sorbent for CO_2 capture has been widely studied, from an experimental point of view for industrial processes [4-6], a kinetic model has been developed by Rouchon et al. [7] and other different models has been yet proposed [5,6,8]. Although, CaO as CO_2 sorbent presents several drawbacks for example a high temperature is required to regenerate the oxide, then, as well the number of carbonation cycles increases the reactivity of CaO toward CO_2 decreases [5].

Recently numerous papers have focused on the synthesis of magnesium oxide with several particle size (nanocrystals, ordered nano- and micro-structures), various morphologies (dots, belts, sheets, plates) [9] and different hierarchical structures 2D and 3D, these materials can be attractive for important applications as a catalyst or catalyst support.

However, few researches revealed the use of MgO as a sorbent for CO_2 [10–14].

From the studies of Fagerlund et al. [10] and Kumar et al. [11] the carbonation of MgO takes place only at high temperature (300°C-350°C) and pressure (10 bar - 20 bar) range in the presence of water vapor (>5%). Otherwise at low or high temperature and atmospheric pressure a small weight gain (less than 8%) can be observed and it is explained by physical or chemical adsorption [12-14]. All studies confirm the significant role of the high surface area and porosity.

Based on these results we are interested to improve the reactivity of MgO towards CO_2 at low temperature and atmospheric pressure by the addition of water vapor and synthesis of mesoporous MgO with high surface area via a simple and safe method.

2. Experimental

2.1 Materials

Two types of MgO samples were used to study the carbonation reaction at low temperature. The first one was prepared by thermal treatment of hydromagnesite ($Mg_5(CO_3)_4(OH)_2 \cdot 4H_2O$) powder provided by central pharmacy of Tunisia. For each experiment hydromagnesite were heated in an alumina crucible under argon flow. Two different heat treatment reactors were used: a) Setaram TAG 16 thermogravimetric analyzer with about about 136 mg of hydromagnesite to study the decomposition reaction and to synthesize MgO powder; and b) a Microcor III PR tube furnace with alumina crucible under argon flow to produce high amount of MgO for textural characterization, using about 600 mg of hydromagnesite. The procedure used in both reactors (i.e. thermobalance and tube furnace) was the same. A recent study [15] of the decomposition reaction of hydromagnesite by in-situ XRD has put in evidence that MgO appears at about 350°C under reducing atmosphere. In order to optimize the thermal treatment and to stabilize a solid phase before the formation of MgO, a thermal treatment program was chosen as follow: for the decomposition reaction to be completed, hydromagnesite was first heated up to 300°C then up to 600°C with a heating rate of 20°C min^{-1}. The temperature remained at 300°C for 3h and at 600°C for 3h to remove residual water and CO_2 molecules. The obtained white powder was noted ‘MgO-T’.

The second type of samples is a commercial MgO powder, delivered by Alfa Aesar with a purity of 99.99 % and was used as a reference material noted ‘MgO-C’.

2.2 Samples characterization

2.2.1 Nitrogen physisorption

The isothermal nitrogen adsorption was employed to measure specific surface areas of both MgO samples. The specific surface area was calculated using the Brunauer-Emmett and Teller (BET) method. The pore volume was also calculated from the adsorbed nitrogen after complete pore condensation ($P/P_0 = 0.9827$) using the ratio of the densities of liquid and gaseous nitrogen. The pore size distribution was calculated using the Barett-Joyner-Halenda (BJH) method. Micrometrics ASAP 2020 was used with N_2 as adsorptive gas at 77 K. About 2 g of sample were weighted in a quartz tube then degassed at 120 °C under vacuum for 8 h to remove adsorbed gases before nitrogen adsorption measurements.

2.2.2Powder XRD

The X-ray diffraction (XRD) patterns of the products was performed using a Siemens D5000 diffractometer with Cu K_α radiation (λ= 1.5406 Å).

2.2.3 ATR-FTIR spectroscopy

Samples were placed face-down on the diamond crystal, and a force manually was applied by pressure tip. FTIR spectra over the 4000-400 cm^{-1} range were recorded by the co-addition of 64 scans with a resolution of 4 cm^{-1}.The entire ATR-FTIR spectra were collected using a Golden Gate Diamond ATR accessory (Bruker Vertex 7).

2.2.4 Raman spectroscopy

Raman spectra were recorded using a Horiba Jobin-Yvon Xplora spectrometer system, equipped with a confocal microscope and a nitrogen-cooled CCD detector, the 532 nm line from a YAG solid was used as the excitation source. The resolution of Raman was set to 4 cm^{-1}.

2.2.5 SEM

Samples before and after carbonation reaction were examined by scanning electron microscopy (SEM - JEOL JSM6400) to compare the morphology of both MgO samples. Samples were placed on an aluminum sampler using a graphite adhesive tab and coated with a thin gold film (≈ 20 nm thick).

2.3 Thermal analysis

The mass change is monitored by means of Mettler Toledo TGA/DSC 1 for CO_2 reaction analyses. The reacting gas mixture contains CO_2, Ar and water vapor in proportions fixed due to mass flow controllers and steam generator (Setaram Wetsys). For each experiment around 7 mg of MgO was loaded and weighted in alumina crucible.

Experiments were designed according to the following protocol: a pretreatment step is carried out at 600°C during one hour under pure argon flow to remove adsorbed gases from MgO. Afterward the temperature was decreased to the reaction temperature in the range 30-50 °C with a heating rate of 20°C min^{-1}, and then the reacting gas mixture was introduced the partial pressure are maintained during the experiment.

In order to produce sufficient quantity of sample to allow surface area and porosimetry analyses after and before carbonation, a tube furnace Microcor III Pr was used, the protocol of experiment is the same as for TG.

3 Results and discussion

3.1 Thermal decomposition of hydromagnesite

3.1.1 Samples characterization

Fig. 1 shows the XRD patterns of both MgO-T and MgO-C.

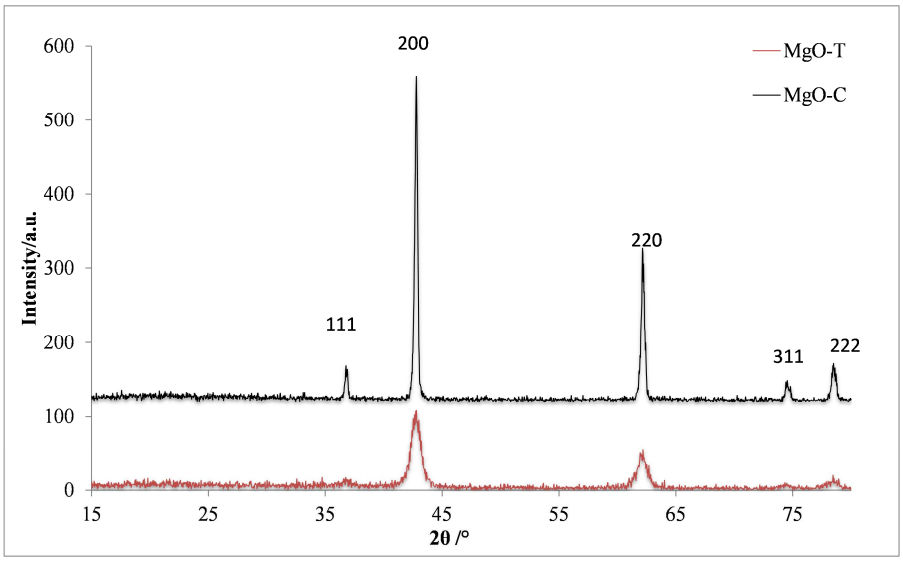

Fig. 1 Powder XRD patterns for MgO-T and MgO-C

MgO-T diffraction peak coincide with those of cubic MgO, indicating the uniform single-phase and cubic in crystal structure existing in this sample. MgO-T peaks are less intensive and broader than those of commercial MgO-C, it can be concluded that the powder is consisted of smaller crystals and the hydromagnesite is completely decomposed into MgO.

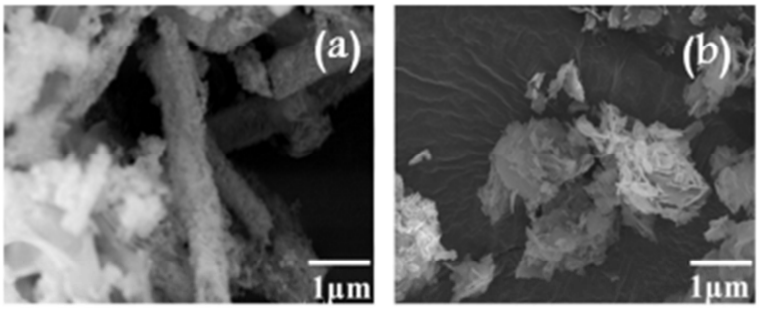

Fig. 2 SEM images of (a) MgO-C and (b) MgO-T

Scanning electron microscope (SEM) images of these samples are provided in Fig. 2, clearly showing the difference in morphology between both magnesium oxide samples. MgO-T displays agglomerated micro sheet particles and exhibited a multiple porous structure whereas MgO-C consists of larger cylindrical particles. From this work and others it can be observed that the morphology of MgO particles could be different and is clearly affected by the type of the precursors and the thermal treatment program. For example, Selvamani et al. [9] produced MgO after calcination of home-made hydromagnesite during 5h in air: for calcination at 450°C, they obtained MgO nano-sheets while for calcination at 550°C MgO has a flower-like structure. Niu et al. [16] have used another precursor, i.e.

magnesium nitrate, and calcination at 500°C during 2h and obtained MgO nanoplates with a specific surface area of 190 $m^2 g^{-1}$. By calcination of home-made nesquehonite under flowing nitrogen up to 400°C, Jauffret at al. [17] reported micrometric particles with needle-like morphology.

Sample	BET surface area /$m^2 g^{-1}$	Pore volume /$cm^3 g^{-1}$	Average pore size /nm
Hydromagnesite	23.1	0.07	14.09
MgO-C	8.7	0.05	23.61
MgO-T	99.3	0.35	11.34
MgO from magnesium nitrate-800°C [12]	250	0.53	5.2
MgO from magnesium carbonate-800°C [13]	29.5	-	-
MgO from $(CH_3COO)_2Mg \cdot 4H_2O$ – 400°C [14]	101	0.175	6.9
MgO from $(CH_3COO)_2Mg \cdot 4H_2O$ – 450°C [14]	99	0.174	7.0
MgO from $(CH_3COO)_2Mg \cdot 4H_2O$ – 500°C [14]	81	0.172	8.4
MgO from $(CH_3COO)_2Mg \cdot 4H_2O$ – 550°C [14]	72	0.150	8.3
MgO from $(CH_3COO)_2Mg \cdot 4H_2O$ – 600°C [14]	53	0.157	11.8

Table 1 Textural properties of MgO-C, MgO-T and hydromagnesite as well as MgO obtained in the literature

Table 1 presents BET specific surface area measurement, pore volume and average pore size of hydromagnesite, MgO-T, and commercially available MgO-C. Synthesized MgO-T has the highest specific surface area (about 100 $m^2 g^{-1}$), about 11 times greater than commercial MgO. Comparison between MgO-T and its precursor, i.e. hydromagnesite, shows that the decomposition leads to an increase of both the specific surface area and the total pore volume which is quite expected in the case of thermal decomposition of solids [18]

The specific surface area values of MgO samples used in the literature for CO_2 sorption are also reported in Table 1: the value of S_{BET} for MgO-T is intermediate among the broad range available from other studies.

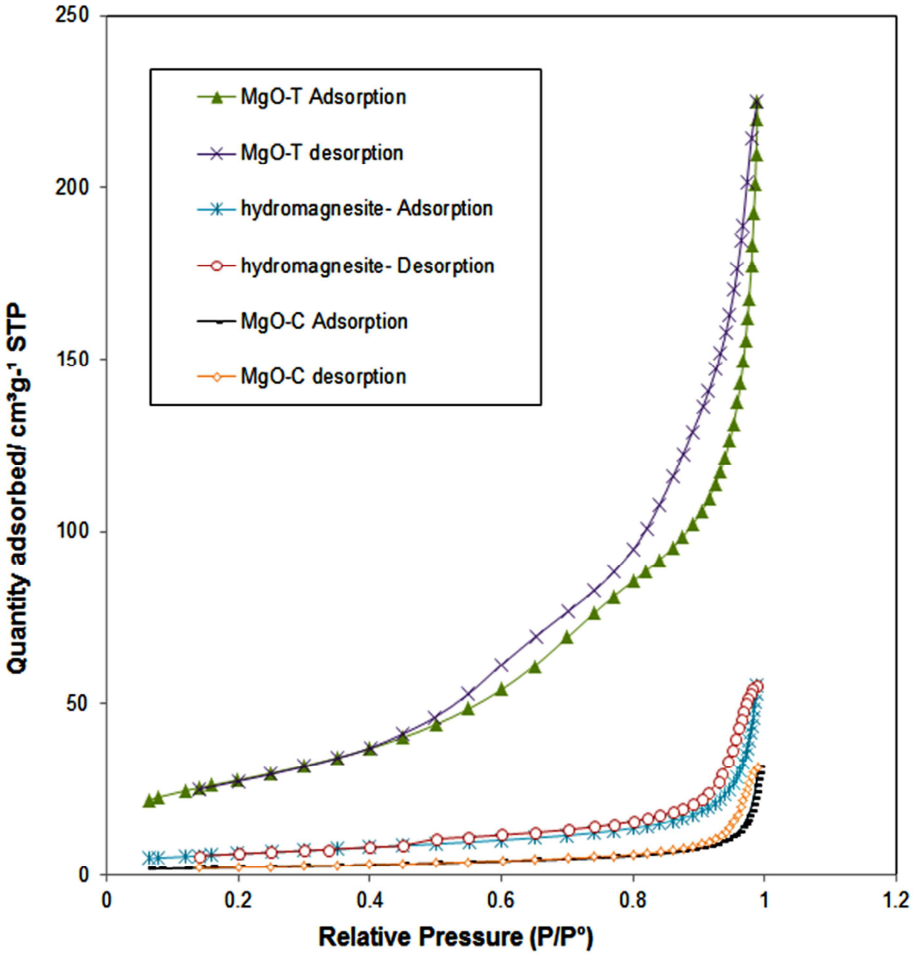

Fig. 3 Nitrogen adsorption-desorption isotherms of both MgO-T and hydromagnesite

Since MgO-T showed a higher porous volume than MgO-C it will be better to have more detailed information about its structure in order to understand the origin of this feature and to use it for CO_2 capture. So the adsorption-desorption isotherms of MgO-T were measured and compared with those of its precursor, i.e. hydromagnesite. The isotherms thus obtained are presented on Figure 3. According to the IUPAC classification [19], these profiles are convex to the p/p° axis indicating type III isotherms, with H3 hysteresis type. Thus, mesopores are probably resulting from crystalline particles aggregation.

Type III isotherms are representative of a specific case, where adsorption at low air-phase concentrations is very little: in this case adsorbate/adsorbate interactions have an important role, so as soon as an island of adsorbate nucleates on the surface, additional adsorption will take place since the adsorbate/adsorbate interactions are strong [20].

MgO-C exhibits very low adsorbed quantity which is in accordance with the low specific surface area measure by the BET method. Moreover the hysteresis loop is very weak indicating a very small number of mesopores in this solid. This confirms that MgO-T present higher pore volume than MgO-C and thus seems to be a better candidate for CO_2 capture.

Pore size distribution has an important role in adsorption process since it can affect the mass transport. Consequently, the pore size distribution was calculated from desorption isotherm presented in Fig. 3 for MgO-T sample and hydromagnesite and results are shown in Fig.4.

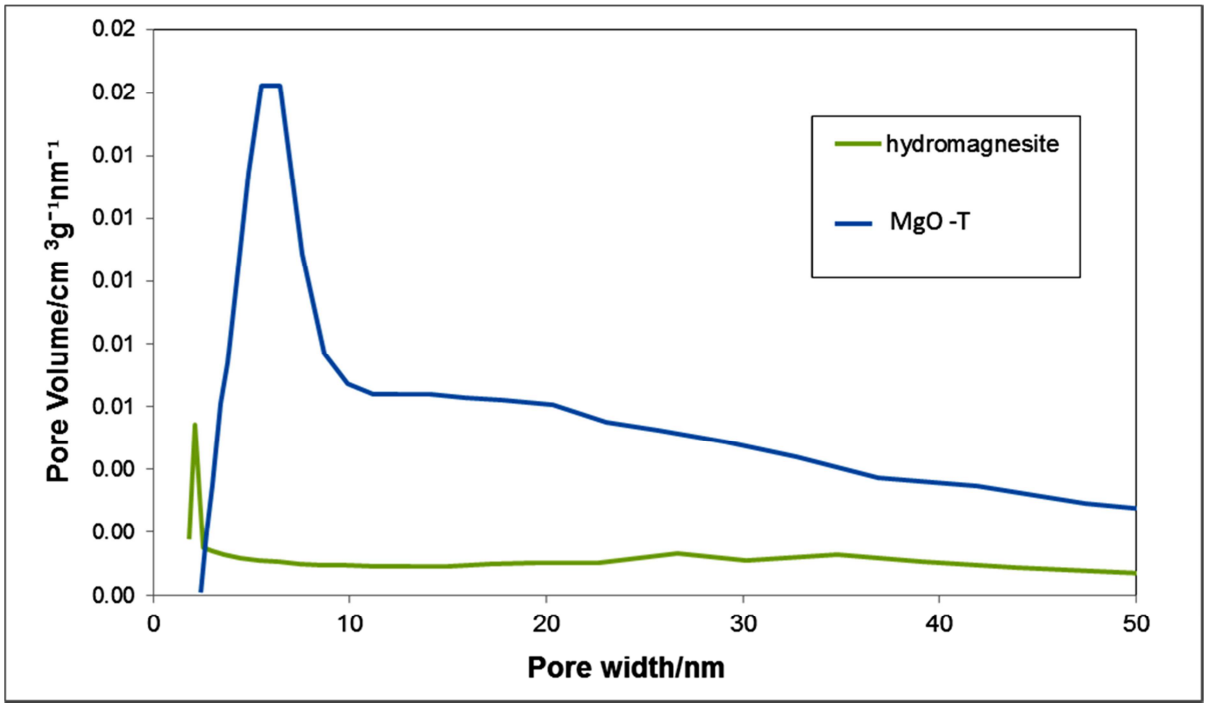

Fig.4 Pore size distribution of hydromagnesite, and MgO-T

From Fig.3 and Fig.4, it can also be seen that isotherms, hysteresis loop, and pore size distribution of both MgO-T and hydromagnesite present the same overall appearance. This indicates that they present quite analogous morphological and textural mesoporous structure. The differences of adsorbed quantities (Fig.3) and in pore volume (Fig.4) as well as the differences of specific surface area and total pore volume (Table 1) and the similarity of the average pore size (Table 1) between both solids seem to indicate that the thermal decomposition of hydromagnesite leads to an increase of the number of mesopores without drastically change their sizes. The morphological similarity is confirmed by means of SEM observations which put in evidence that hydromagnesite and MgO-T exhibit micro-sheet assembly in flower-like structure (Figs. 5a and 5b). Moreover, Figs. 5c and 5d reveal that MgO-T individual particle can be schematized by a square plate with a length of about 1.5 µm and a thickness of about 100 nm.

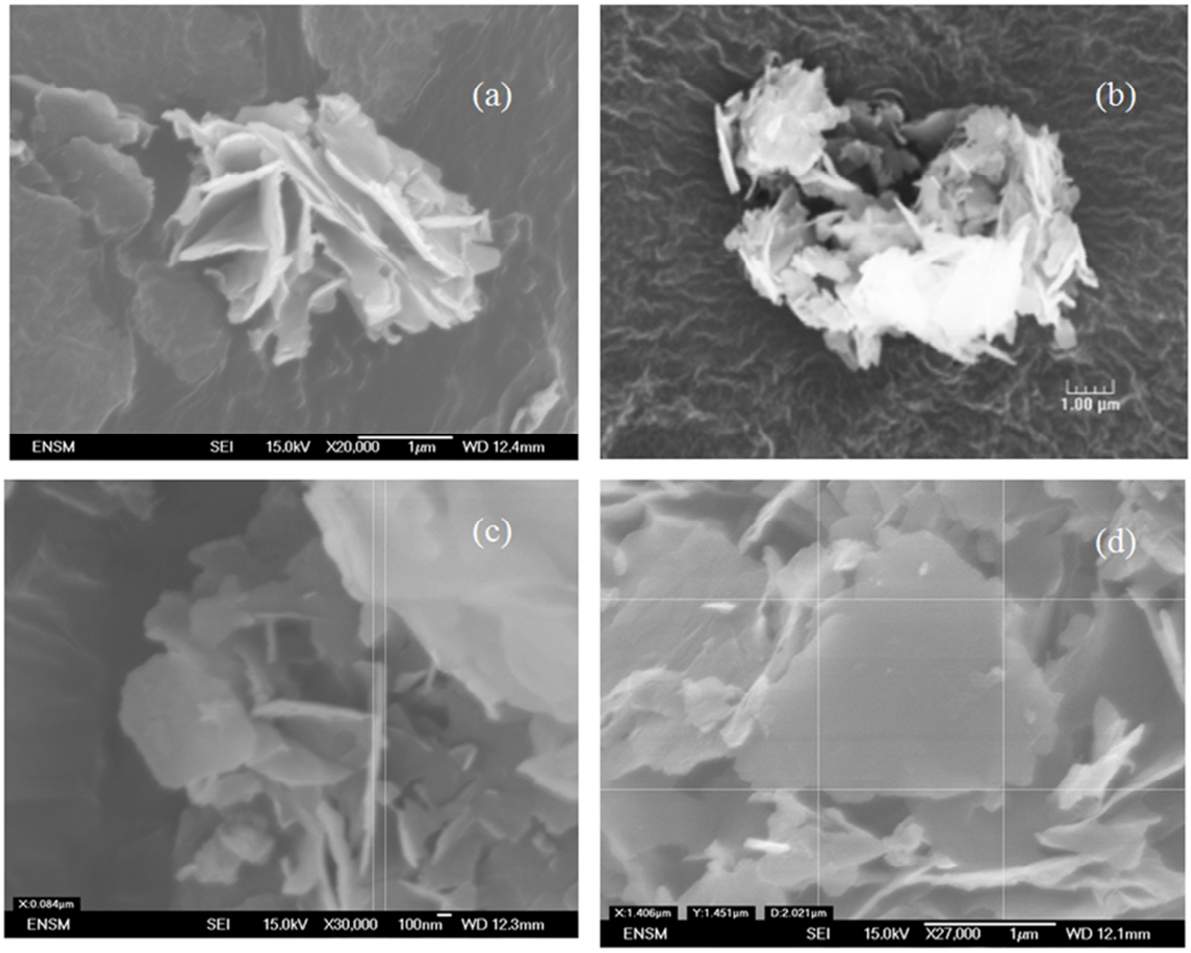

Fig. 5 SEM-image of (a) MgO-T flower like aggregate, (b) hydromagnesite and (c-d) individual MgO-T crystal dimension

Using these dimensions, specific external surface area of MgO-T individual particle can be recalculated according to:

$$S_{spe} = \frac{2\,a^2 + 4\,a\,e}{\rho\,a^2\,e} \qquad (1)$$

with ρ the density of MgO equal to 3.58 g cm^{-3},a and e the length and the thickness of the individual particle respectively.

Thus the specific external surface area of an individual MgO-T particle is about S_{spe}= 6.3 m^2 g^{-1}. This value is smaller than BET surface area measurement (S_{BET} = 99.3 m^2 g^{-1} - see Table 1) which confirms the mesoporous structure of the particle.

Thus the as-obtained MgO powder (MgO-T) presents greater specific surface area and pore volume than the commercial powder (MgO-C). Moreover, the porosity of the MgO-T particles seems to be mostly constituted by mesopores. In consequence MgO-T appears as a better candidate than commercial MgO for CO_2 capture application.

3.1.2 Thermal behavior of hydromagnesite

In Figure 6 are reported TG and DTG curves obtained for the thermal decomposition of hydromagnesite ($Mg_5(CO_3)_4(OH)_2.4H_2O$) sample recorded using the protocol described in section 2.1. The total mass loss is about 58.6% and the mass-loss curve (Fig. 6a) exhibits four processes corresponding to the four peaks observed on the DTG signal (Fig. 6b). The first mass loss (first DTG peak) of about 2.7% of the initial sample mass occurs before 100°C and is due to water desorption from the surface of hydromagnesite sample. The three following mass-losses are linked with the thermal decomposition of hydromagnesite. The first one occurs between 100 and 300°C and is equal to about 14.9% The largest mass loss (about 32.3%) corresponding to the third DTG peak begins at about 320°C. Finally a final mass loss of about 8.7% takes place at about 480°C. These mass losses have to be interpreted as the removal of CO_2 and H_2O gaseous molecules. The first mass loss (about 14.9%) corresponds to the mass loss of four water molecules of crystallization (theoretical mass loss of 15.4%). The intermediate solid at 300°C is thus anhydrous $Mg_5(CO_3)_4(OH)_2$. The second mass loss of about 32.3% corresponds to the removal of three carbon dioxide molecules and one water molecule which theoretically lead to a mass loss of 32.1%. Finally, the third mass loss corresponds to the removal of one CO_2 molecule.

Thus a reaction scheme can be proposed, as detailed in Table 2.

N°	Reaction	Theoretical mass loss/%	Experimental mass loss/%
1	$Mg_5(CO_3)_4(OH)_2 \cdot 4H_2O \rightarrow Mg_5(CO_3)_4(OH)_2 + 4H_2O$	15.4%	14.9%
2	$Mg_5(CO_3)_4(OH)_2 \rightarrow MgCO_3 + 4MgO + 3CO_2 + H_2O$	32.1%	32.3%
3	$MgCO_3 \rightarrow MgO + CO_2$	9.4%	8.7%
Total	$Mg_5(CO_3)_4(OH)_2 \cdot 4H_2O \rightarrow 5MgO + 4CO_2 + 5H_2O$	56.9%	55.9%

Table 2 The reaction scheme

Analysis of the reaction scheme from the literature about hydromagnesite decomposition reaction doesn't allow to express a common scheme. If the presence of CO_2 in the atmosphere of decomposition is known to change the reaction mechanism [21-26], Hollingbery et al. [27] made a review on the thermal decomposition of hydromagnesite and have shown that under inert gas the decomposition has been described in two or three steps. The decomposition mechanism reported in our work is in three steps detailed in Table 2. Todor [28] has also proposed a decomposition mechanism in three steps but the nature of the second step differs from our results: 1) the first step is similar and corresponds to the dehydration of hydromagnesite with the release of four water molecules; 2) our second step is the decomposition reaction of anhydrous magnesium carbonate hydroxide and leads to the formation of one molecule of magnesium carbonate and four molecules of MgO with production of three CO_2 molecules and one H_2O molecule (whereas Todor has proposed that this thermal decomposition leads to two molecules of magnesium carbonate and three molecules of MgO with the production of two CO_2 molecules and one H_2O molecule) ; 3) finally the third step corresponds to the decomposition reaction of magnesium carbonate to produce MgO and CO_2 in both mechanisms.

Hollingbery et al. [27] performed DSC measurements in air and obtained three endothermic peaks which are characteristic of three reaction steps (an exothermic peak is also obtained and was attributed to carbonate crystallization). Nevertheless, they didn't compare the heat flow for each step with the mechanism proposed by Todor.

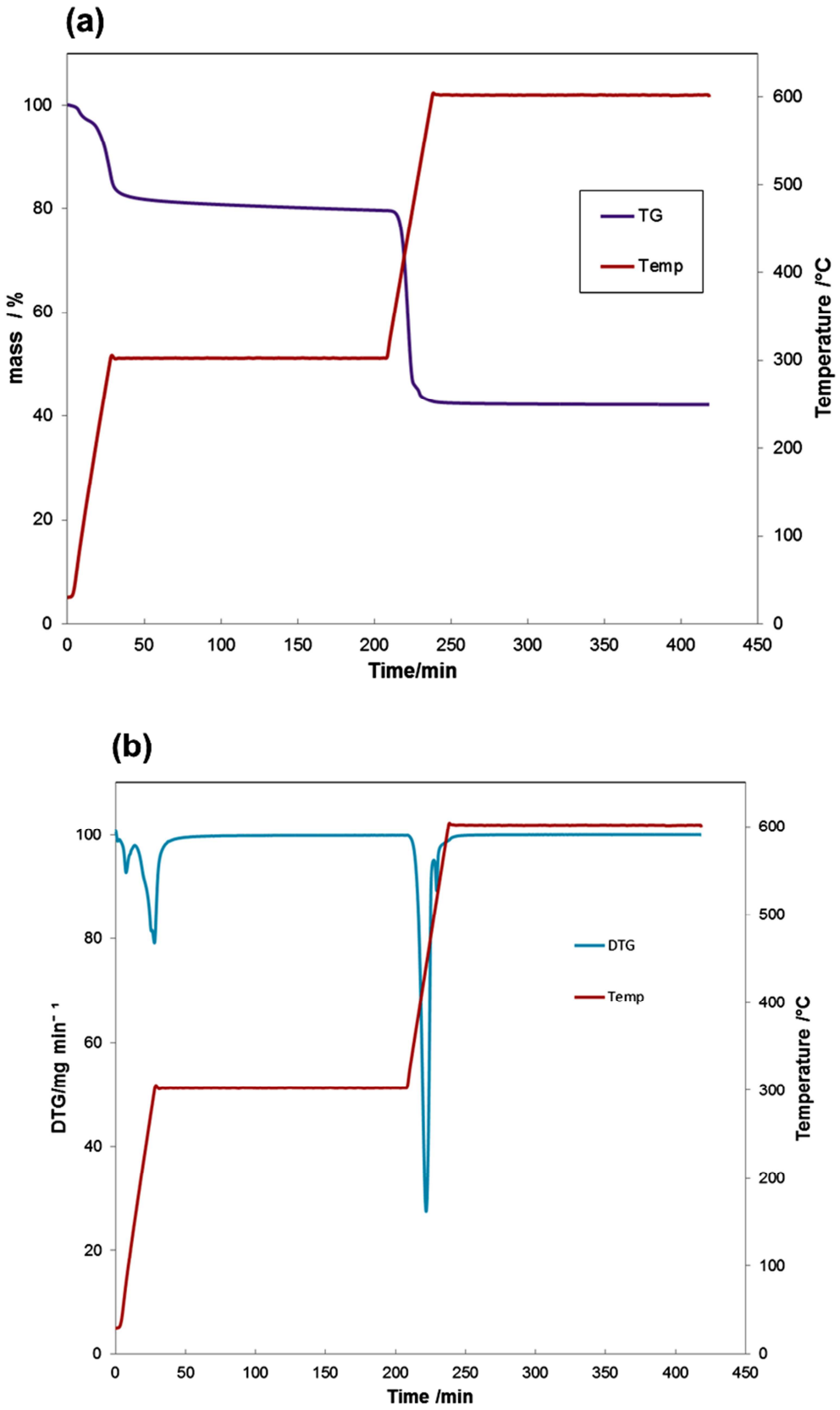

Fig.6 (a) TG profile and (b) DTG profile of as prepared MgO micro-sheets

3.2 Reaction of MgO with CO_2

As it has been shown that carbonation remains very low for MgO samples with low specific surface area even under high CO_2 pressure (10 bars) [11], our carbonation tests were performed using the home-made MgO-T exhibiting a higher specific surface area and pore volume.

3.2.1 Influence of water vapor

To evaluate the sorption performance of the synthesized MgO-T in the presence and absence of steam at high and low temperatures, the CO_2 uptake capacity was examined using a thermogravimetric analyzer (TG) at P_{tot} = 1 bar, P_{CO2} = 600 mbar and P_{H2O} = 15 mbar. The corresponding TG curves are shown in Fig.7 and Fig.8. It can be observed that the mass gain is more important and faster in the presence of steam than in a dry CO_2 atmosphere. Indeed at 30°C the mass gain reaches about 11% of the initial mass in the case of wet CO_2 whereas is doesn't exceed 2% of the initial mass under dry CO_2. This behavior remains true at higher temperature as shown in Figure 8 at 300°C.

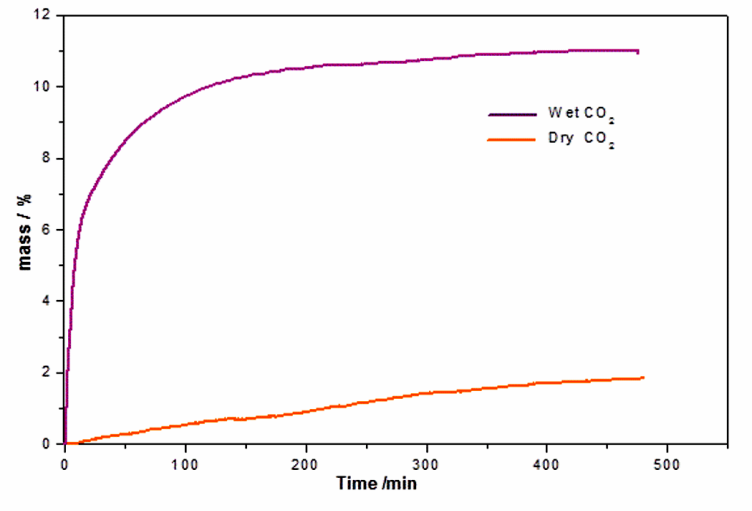

Fig.7 Comparison between carbonation (30°C, P_{tot} = 1 bar, PCO_2 = 600 mbar) with and without water vapor (in the case of wet CO_2, the water vapor pressure is fixed to 15 mbar)

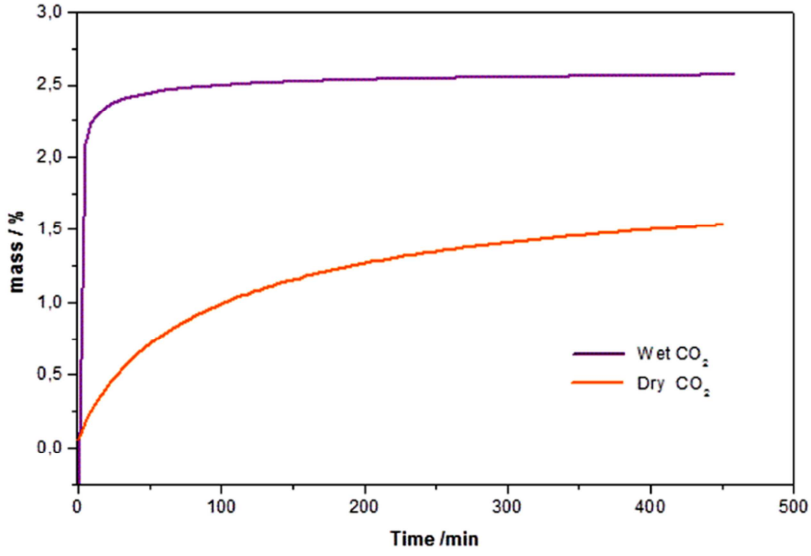

Fig. 8 Comparison between carbonation (300°C, P_{tot} = 1 bar, PCO_2 = 600 mbar) with and without water vapor (in the case of wet CO_2, the water vapor pressure is fixed to 15 mbar)

It can be concluded that MgO is much more reactive in humid CO_2 which is in accordance with the results of Fargelund et al. [10]. In the following, reactivity of CO_2 with MgO will be studied only in presence of water vapor.

3.2.2 Influence of temperature

CO_2 uptake profile over mesoporous MgO at 30, 50 and 300 °C monitored by TG for P_{CO2}= 600 mbar and P_{H2O} = 15 mbar are shown in Fig. 9. It can be seen that the total CO_2 uptake increases when temperature decreases, so the most important uptake capacity was measured at T= 30 °C. This value can reach 11% and is 5 times higher than that of the uptake capacity in the same condition at high temperature T= 300°C.

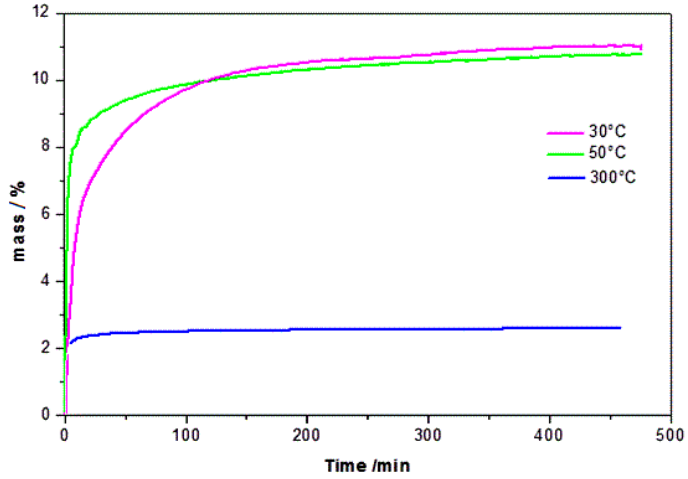

Fig.9 TG curves of CO_2 sorption on MgO-T at various temperatures, P_{CO2} = 600 mbar and P_{H2O} = 15 mbar

In order to distinguish if the mass gain is due to physisorption, chemisorption (surface carbonates) or carbonation (bulk carbonates), ATR-FTIR spectrums were recorded during the reaction at different reaction time (from 15 minutes to 24h) and are shown in Fig. 10. Identification of the absorption bands detected on our samples was made thanks to literature data [29-32].

The sample reacted during 15 minutes exhibits:

- The asymmetric stretching vibration of carbonate ion υ_3 is observed as a large band splitted into two bands at 1420 cm^{-1} and at 1480 cm^{-1}.
- A weak band is observed at 860 cm^{-1} and is assigned to the CO_3^{2-} out-of-plane bend (υ_2).
- The large band at 3300 cm^{-1} attributed to water of crystallization, in addition to a broad shoulder at 1650 cm^{-1} due to O-H bending of water (υ_2).
- The background noise in the signal between 1900 and 2200 cm^{-1} is assigned to atmospheric CO_2.

After 18 and 24 hours of reaction, a low intensity band appears at 1098 cm^{-1} assigned to the symmetric stretching vibration of carbonate ion υ_1,the intensity of bands increases, and the doublet at 1420 cm^{-1} and 1480 cm^{-1} became one single large band centered at 1420 cm^{-1} as shown in Fig. 11.

Based on the results of the literature, IR absorption bands at 1420 cm^{-1}, 1098 cm^{-1} and 860 cm^{-1} indicate the formation of bulk carbonates phase [31-34], and those at 3300 cm^{-1} and 1650 cm^{-1} indicate that the synthesized material is a hydrated carbonate [31].

However the absence of hydroxide's characteristic band around 3600 cm^{-1} and hydrogen carbonate's band at 1220 cm^{-1} [35] confirms that the synthesized material could be nesquehonite $MgCO_3.3H_2O$ or lansfordite $MgCO_3.5H_2O$. The band at 1098 cm^{-1} is in good agreement with the value of 1099 cm^{-1} reported by [29] for nesquehonite.

Moreover lansfordite is thermodynamically unstable and always accompanied with other magnesium carbonate hydrates at ambient temperature and atmospheric pressure [36]. Nesquehonite is the most stable phase under ambient conditions in the phase diagram system $MgO-H_2O-CO_2$, the most probable solid phase formed should be nesquehonite [37, 38].

Characterization with both Infrared and Raman spectroscopy gives sensitive tests for distortion of the carbonate units [31], so the multiplicity observed for the antisymmetric stretching mode before 24 hours of reaction was due to the distortion of CO_3^{2-}, when the quantity of the new carbonated hydrated phase increases in the material the distortion of CO_3^{2-} decreases which's manifested by the transformation of the doublet at 1420 cm^{-1} and at 1480 cm^{-1} to a single centered band at 1420 cm^{-1}.

According to literature [39] the existence of υ_1 in the IR spectra indicates that the structure is no more centrosymmetric, which confirms the change from the periclase structure (CFC) to another structure.

Knowing that nesquehonite has a more complicated structure consisting of 2-dimensional ribbons of coplanar $MgCO_3$ besieged by water molecules, two-thirds of which are axially coordinated to the magnesium ions while one-third hydrogen bonded to the carbonate groups along the edges of the flat ribbons, hydrogen bonding is not awaited to extremely affect the CO_3^{2-} internal vibrations in this structure [37, 39], which is in accordance with the change of IR spectra after 18 and 24 hours of reaction.

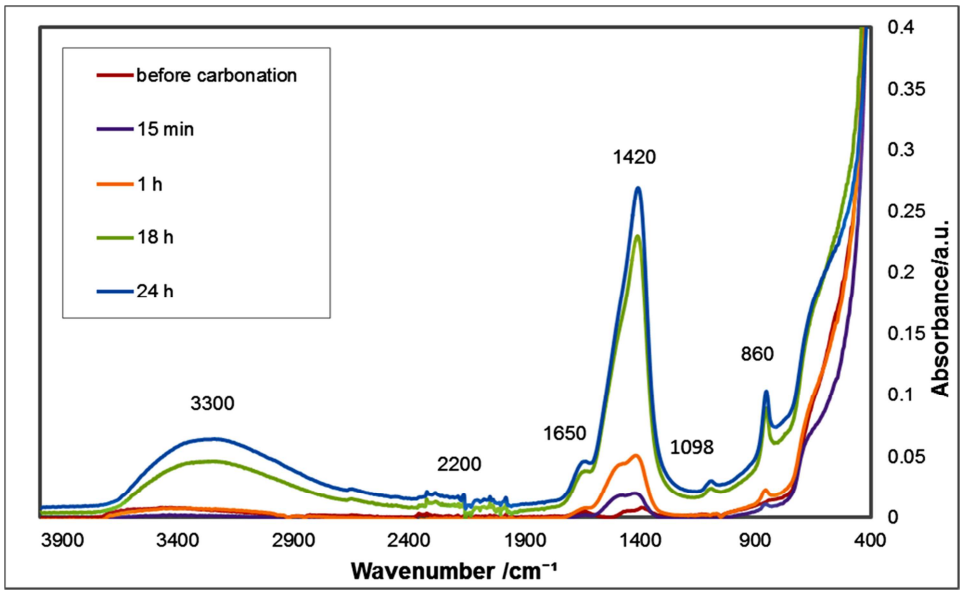

Fig. 10 Infrared spectra of MgO before carbonation, after 15 minutes,1 hour, 18 hours and 24 hours of carbonation **(T= 30°C, P_{CO2}= 500 mbar et P_{H2O}= 15 mbar)**

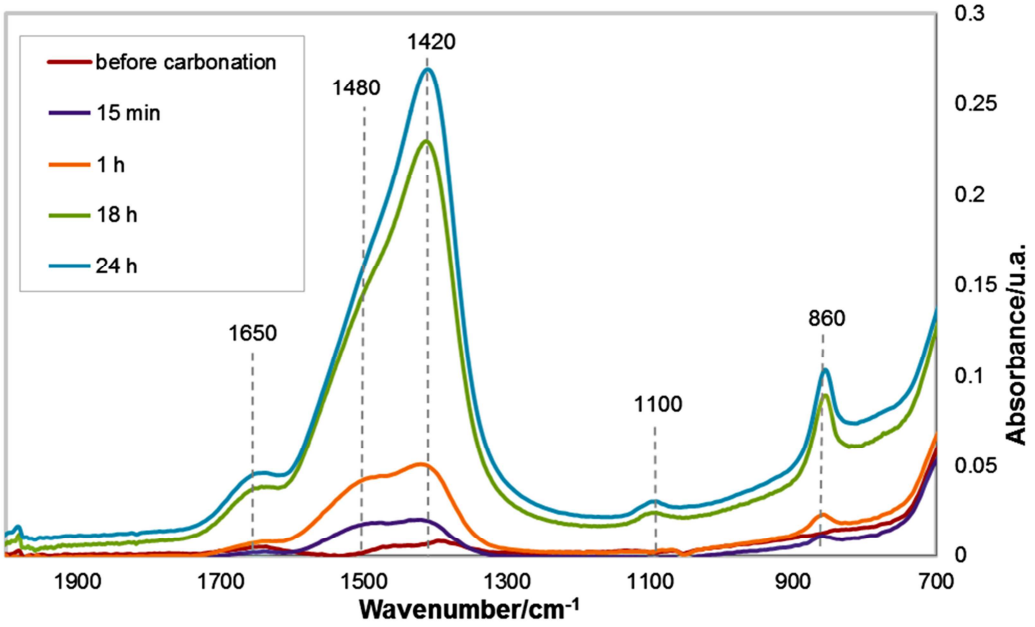

Fig. 11 Infrared spectra of MgO before carbonation, after 15 minutes,1 hour, 18 hours and 24 hours of carbonation **(T= 30°C, P_{CO2}=500 mbar et P_{H2O}=15 mbar)**

Raman spectrum (Fig. 12) confirms the formation of a carbonated phase. This spectrum exhibits only the symmetric stretching vibration of carbonate ion υ_1 (strong in Raman) for the product obtained after 24 hours of reaction, whereas for other materials ($MgO\text{-}CO_2\text{-}H_2O$ system reaction's product for carbonation time less than 18h) internal modes didn't appear which can be probably due to structural disorder in these materials.

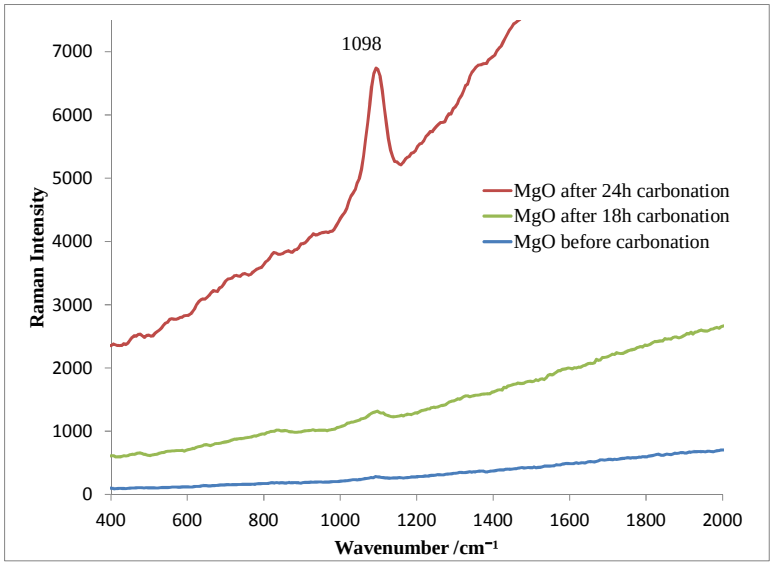

Fig. 12 Raman spectra of MgO before carbonation and after carbonation during 18h and 24h **(T= 30°C, P_{CO2}= 500 mbar et P_{H2O}= 15 mbar)**

Thus Infrared and Raman spectroscopies allow to determine the formation of the nesquehonite phase $MgCO_3.3H_2O$ during carbonation reaction of mesoporous MgO at 30°C under atmosphere containing carbon dioxide and water vapor.

By considering the reaction $MgO(s) + CO_2(g) + 3H_2O(g) \rightarrow MgCO_3 \cdot 3H_2O(s)$, it is possible to transform the mass gain during reaction into fractional conversion α according to :

$$\alpha = \frac{m - m_0}{\Delta m_{th}}$$

with m the powder mass at the time t, m_0 the powder mass before carbonation and Δm_{th} the theoretical mass gain given by:

$$\Delta m_{th} = \frac{m_0}{M_{MgO}} M_{CO_2}$$

with M_{MgO} the molar mass of MgO, equal to 40.30 g mol^{-1} and M_{CO2} the molar mass of CO_2 equal to 44 g mol^{-1}

The carbonation reaction operated during 24h at 30°C under P(CO_2) = 500 mbar and P(H_2O = 15 mbar lead to a fractional conversion of 0.54.

In order to determine the change of textural characteristics occurring during carbonation, samples of MgO and MgO after reaction during 24h at T=30°C, P_{CO2} = 500 mbar and P_{H2O}=15 mbar were examined by means of scanning electron microscope, specific surface area measurement (BET method) and porosity analyze (BJH method).

The specific surface area and the pore volume for both samples are presented in Table 3. A significant decrease in values after 24h carbonation is observed since both specific surface area and pore volume decrease by a factor 10. Moreover, comparison of MgO pore size distribution (Fig. 13) before reaction, after 2 and 24 hours of reaction (α = 0.09 and 0.54 respectively), shows that all mesoporous volume tends to decrease with carbonation and seems to disappear when reaction conversion overcomes 50%. These results indicate the important role of CO_2 uptake on the particle structure: during carbonation, as far as the fractional conversion increases, the size of the dense particles increases and the porosity between them tends to disappear. Such changes are not surprising since the volume expansion due to the MgO–$MgCO_3$.3H_2O transformation is quite important (the ratio of the molar volumes $MgCO_3$.3H_2O/MgO is equal to 6.68).

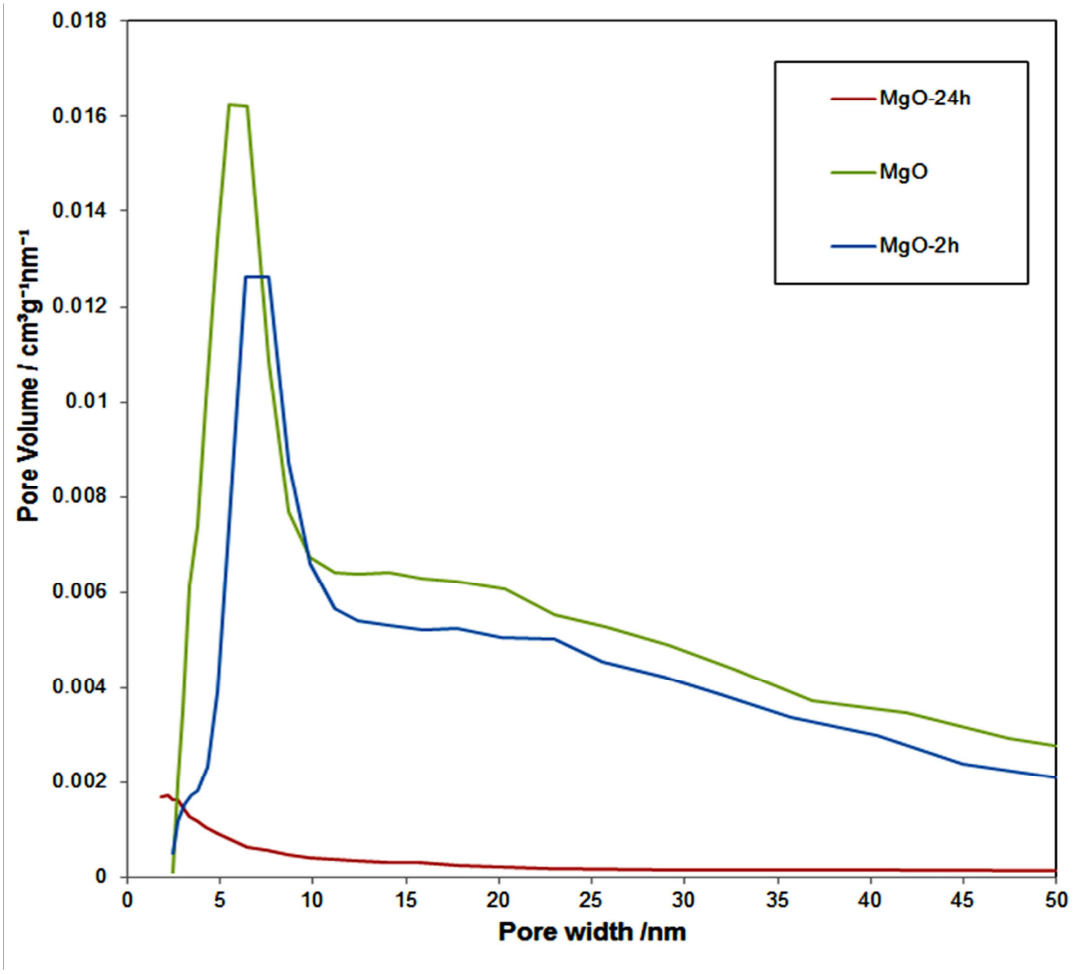

Fig.13 Pore size distribution of synthesized MgO-T sample before reaction and MgO-T samples after 2 hours and 24 hours of reaction

Sample	BET surface area /m² g^{-1}	Pore volume /cm^3 g^{-1}
MgO before carbonation	99.3	0.35
MgO after 2h carbonation	61.1	0.28
MgO after 24h carbonation	10.3	0.037

Table 3 Surface properties of MgO after and before carbonation

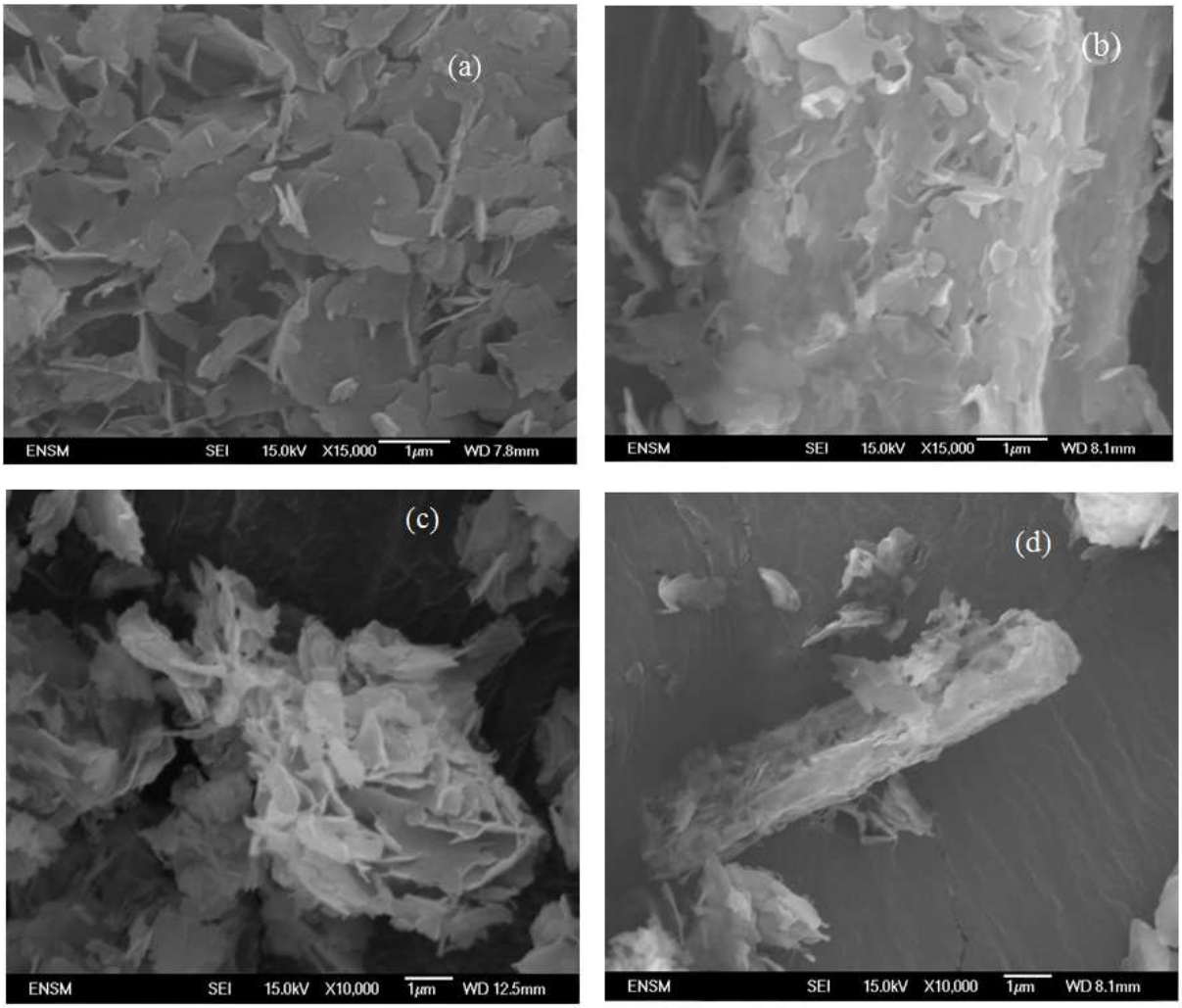

Fig. 14 SEM images of MgO before (a and c) and after carbonation (b and c) **at T= 30°C, P_{CO2}= 500 mbar and P_{H2O}= 15 mbar**

Fig. 14 shows the morphological change of the particle and aggregate surface before (Figs 14.a and c) and after 18 hours of carbonation reaction. It appears that micro-sheets of MgO were welded together forming a rough surface after carbonation (Fig 14.b). The aggregate is no more flower-like shaped (Fig 14.c) but needle shaped (Fig 14.d). The shape of the particles after carbonation tends to confirm that the solid product is $MgCO_3 .3H_2O$. Indeed nesquehonite crystals have been observed during several studies and the morphology was always reported to be needle-like. The authors have synthesized nesquehonite by means of precipitation from $MgCl_2.6H_2O$ and Na_2CO_3 aqueous solutions [17, 24, 40], precipitation from $MgCl_2.6H_2O$ and aqueous ammonia with sparged CO_2 [41] or precipitation from $Mg(OH)_2$ aqueous solution with sparged CO_2 [42]. Nevertheless to our knowledge there is no work reporting the synthesis of $MgCO_3.3H_2O$ by solid-gas reaction between mesoporous MgO powder and CO_2 in the presence of water vapor.

4 Conclusion

Mesoporous MgO powder has been synthesized via hydromagnesite thermal decomposition. The MgO powder thus obtained exhibits a fairly large specific surface area and a high total pore volume compared with commercial magnesium oxide powder.

MgO carbonation reaction study was carried out at several experimental conditions by means of thermogravimetry analysis. We have shown that the carbonation of mesoporous MgO is possible even at room temperature and with CO_2 pressure less than the atmospheric pressure which means that CO_2 capture using MgO is possible in these conditions. Nevertheless the presence of water vapor is required in order to enhance carbonation reaction. Moreover IRTF spectroscopy and Raman spectroscopy allowed to determine that the reaction of MgO with wet CO2 leads to the formation of nesquehonite $MgCO_3.3H_2O$. Finally the best result was obtained at T= 30°C, P_{CO2}= 500 mbar and P_{H2O}= 15 mbar. In these conditions 54% of MgO was converted into $MgCO_3.3H_2O$.

References

1. Intergovernmental Panel on Climate Change, Edenhofer O, editors. Climate change 2014: mitigation of climate change: Working Group III contribution to the Fifth Assessment Report of the Intergovernmental Panel on Climate Change. New York, NY: Cambridge University Press; 2014. 1435 p.

2. SEIFRITZ W. CO_2 disposal by means of silicates. Nature. 1990 Jun 7;345(6275):486–486.

3. Kumar S, Saxena SK. A comparative study of CO_2 sorption properties for different oxides. Mater Renew Sustain Energy (2014) 3: 30. https://doi.org/10.1007/s40243-014-0030-9

4. Rouchon L, Favergeon L, Pijolat M. Analysis of the kinetic slowing down during carbonation of CaO by CO_2. J Therm Anal Calorim. 2013 Sep;113(3):1145–55.

5. Bouquet E, Leyssens G, Schönnenbeck C, Gilot P. The decrease of carbonation efficiency of CaO along calcination–carbonation cycles: Experiments and modelling. Chem Eng Sci. 2009 May;64(9):2136–46.

6. Bhatia SK, Perlmutter DD. Unified treatment of structural effects in fluid-solid reactions. AIChE J. 1983;29(2):281–289.

7. Rouchon L, Favergeon L, Pijolat M. New kinetic model for the rapid step of calcium oxide carbonation by carbon dioxide. J Therm Anal Calorim. 2014 Jun;116(3):1181–8.

8. Sun P, Grace JR, C. Jim Lim, Anthony EJ. A discrete-pore-size-distribution-based gas–solid model and its application to the reaction. Chem Eng Sci. 2008 Jan;63(1):57–70.

9. Selvamani T, Sinhamahapatra A, Bhattacharjya D, Mukhopadhyay I. Rectangular MgO microsheets with strong catalytic activity. Mater Chem Phys. 2011 Oct;129(3):853–61.

10. Fagerlund J, Highfield J, Zevenhoven R. Kinetics studies on wet and dry gas–solid carbonation of MgO and $Mg(OH)_2$ for CO_2 sequestration. RSC Adv. 2012;2(27):10380.

11. Kumar S, Saxena SK, Drozd V, Durygin A. An experimental investigation of mesoporous MgO as a potential pre-combustion CO_2 sorbent. Mater Renew Sustain Energy (2015) 4: 8. https://doi.org/10.1007/s40243-015-0050-0

12. Bhagiyalakshmi M, Lee JY, Jang HT. Synthesis of mesoporous magnesium oxide: Its application to CO_2 chemisorption. Int J Greenh Gas Control. 2010 Jan;4(1):51–6.

13. Torres-Rodríguez DA, Pfeiffer H. Thermokinetic analysis of the MgO surface carbonation process in the presence of water vapor. Thermochim Acta. 2011 Mar;516(1–2):74–8.

14. Song G, Ding Y-D, Zhu X, Liao Q. Carbon dioxide adsorption characteristics of synthesized MgO with various porous structures achieved by varying calcination temperature. Colloids Surf Physicochem Eng Asp. 2015 Apr;470:39–45.

15. Lin Y, Zheng M, Ye C, Power IM. Thermogravimetric analysis–mass spectrometry (TGA–MS) of hydromagnesite from Dujiali Lake in Tibet, China. J Therm Anal Calorim. 2018 Sep;133(3):1429–37.

16. Niu H, Yang Q, Tang K, Xie Y. A simple solution calcination route to porous MgO nanoplates. Microporous Mesoporous Mater. 2006 Nov;96(1–3):428–33.

17. Jauffret G, Morrison J, Glasser FP. On the thermal decomposition of nesquehonite. J Therm Anal Calorim. 2015 Nov;122(2):601–9.

18. Koga N., in *Handbook of Thermal Analysis and Calorimetry*, eds. S. Vyazovkin, N. Koga and C. Schick, Elsevier, Amsterdam, 2nd edn., 2018, vol. 6, ch. 6, pp. 213-251.

19. Sing K, Everett D, Haul R, Moscou L, Pierotti R, Rouquerol J, et al. Reporting physisorption data for 1, 0x10-3 1, 2x10-3 1, 4x10-3 1, 6x10-3 1, 8x10-3 2, 0x10-3-8-6-4-2 0 2 4-1 K) I II III gas/solid systems with special reference to the determination of surface area and porosity. Pure Appl Chem. 1985;57:603–19.

20. Tiffonnet A-L, Blondeau P, Allard F, Haghighat F. Sorption isotherms of acetone on various building materials. Indoor Built Environ. 2002;11(2):95–104.

21. Sawada Y, Uematsu K, Mizutani N, Kato M. Thermal decomposition of hydromagnesite $4MgCO_3 \cdot Mg(OH)_2 \cdot 4H_2O$. J Inorg Nucl Chem. 1978;40(6):979–982.

22. Sawada Y, Uematsu K, Mizutani N, Kato M. Thermal decomposition of hydromagnesite $4MgCO_3$-$Mg(OH)_2$-$4H_2O$ under different partial pressures of carbon dioxide. Thermochim Acta. 1978;27(1–3):45–59.

23. Sawada Y, Yamaguchi J, Sakurai O, Uematsu K, Mizutani N, Kato M. Thermogravimetric study on the decomposition of hydromagnesite $4MgCO_3 \cdot Mg(OH)_2 \cdot 4H_2O$. Thermochim Acta. 1979;33:127–140.

24. Sawada Y, Yamaguchi J, Sakurai O, Uematsu K, Mizutani N, Kato M. Thermal decomposition of basic magnesium carbonates under high-pressure gas atmoshpheres. Thermochim Acta. 1979;32(1–2):277–291.

25. Sawada Y, Yamaguchi J, Sakurai O, Uematsu K, Mizutani N, Kato M. Isothermal differential scanning calorimetry on an exothermic phenomenon during thermal decomposition of hydromagnesite $4MgCO_3 \cdot Mg(OH)_2 \cdot 4H_2O$. Thermochim Acta. 1979;34(2):233–237.

26. Padeste C, Oswald HR, Reller A. The thermal behaviour of pure and nickel-doped hydromagnesite in different atmospheres. Mater Res Bull. 1991;26(12):1263–1268.

27. Hollingbery LA, Hull TR. The thermal decomposition of huntite and hydromagnesite—A review. Thermochim Acta. 2010 Sep;509(1–2):1–11.

28. Todor D. Thermal analysis of minerals. Abacus press. 1976;

27. Coleyshaw EE, Crump G, Griffith WP. Vibrational spectra of the hydrated carbonate minerals ikaite, monohydrocalcite, lansfordite and nesquehonite. Spectrochim Acta A Mol Biomol Spectrosc. 2003 Aug;59(10):2231–9.

28. Frost RL, Palmer SJ. Infrared and infrared emission spectroscopy of nesquehonite $Mg(OH)(HCO_3)\cdot 2H_2O$–implications for the formula of nesquehonite. Spectrochim Acta A Mol Biomol Spectrosc. 2011 Apr;78(4):1255–60.

29. Frost RL, Dickfos M. Hydrated double carbonates – A Raman and infrared spectroscopic study. Polyhedron. 2007 Sep;26(15):4503–8.

30. Edwards HGM, Villar SEJ, Jehlicka J, Munshi T. FT–Raman spectroscopic study of calcium-rich and magnesium-rich carbonate minerals. Spectrochim Acta A Mol Biomol Spectrosc. 2005 Aug;61(10):2273–80.

31. Frost RL, Bahfenne S, Graham J. Raman spectroscopic study of the magnesium-carbonate minerals-artinite and dypingite. J Raman Spectrosc. 2009 Aug;40(8):855–60.

32. Cornu D, Guesmi H, Krafft J-M, Lauron-Pernot H. Lewis Acido-Basic Interactions between CO_2 and MgO Surface: DFT and DRIFT Approaches. J Phys Chem C. 2012 Mar 22;116(11):6645–54.

33. Jin F, Al-Tabbaa A. Evaluation of novel reactive MgO activated slag binder for the immobilisation of lead and zinc. Chemosphere. 2014;117:285–94.

34. Yin W, Wang Y, Ji Q, Yao J, Hou Y, Wang L, et al. Synthesis and formation mechanism of micro/nano flower-like MgCO3·5H2O. Int J Miner Metall Mater. 2014 Mar;21(3):304–10.

35. Chaka AM, Felmy AR. Ab Initio Thermodynamic Model for Magnesium Carbonates and Hydrates. J Phys Chem A. 2014 Sep 4;118(35):7469–88.

36. Hill RJ, Canterford JH, Moyle FJ. New data for lansfordite. Miner Mag. 1982;46(341):453–457.

37. Farmer VC. The infrared spectra of minerals. London: Mineralogical society London SW7 5 HR; 1974.

38. Kloprogge JT, Martens WN, Nothdurft L, Duong LV, Webb GE. Low temperature synthesis and characterization of nesquehonite. J Mater Sci Lett. 2003;22(11):825–829.

40. Ferrini V, De Vito C, Mignardi S. Synthesis of nesquehonite by reaction of gaseous CO_2 with Mg chloride solution: Its potential role in the sequestration of carbon dioxide. J Hazard Mater. 2009 Sep;168(2–3):832–7.

41. Hopkinson L, Kristova P, Rutt K, Cressey G. Phase transitions in the system MgO–CO_2–H_2O during CO_2 degassing of Mg-bearing solutions. Geochim Cosmochim Acta. 2012 Jan;76:1–13.